

Doping stability and opto-electronic performance of chemical vapour deposited graphene on transparent flexible substrates

Moon H. Kang¹, William I. Milne^{1,2}, Matthew T. Cole¹

¹Electrical Engineering Division, Department of Engineering, University of Cambridge, 9 JJ Thomson Avenue, Cambridge CB3 0FA, UK

²Department of Information Display, Kyung Hee University, Seoul 130-701, Korea
 E-mail: mtc35@cam.ac.uk

Abstract: The primary barrier to wider commercial adoption of graphene lies in reducing the sheet resistance of the transferred material without compromising its high broad-band optical transparency, ideally through the use of novel transfer techniques and doping strategies. Here, chemical vapour deposited graphene was uniformly transferred to polymer supports by thermal and ultraviolet (UV) approaches and the time-dependent evolution of the opto-electronic performance was assessed following exposure to three kinds of common dopants. Doping with FeCl₃ and SnCl₂ showed minor, and notably time unstable, enhancement in the $\sigma_{\text{opt}}/\sigma_{\text{dc}}$ figure of merit, while AuCl₃-doping markedly reduced the sheet resistance by 91.5% to 0.29 k Ω /sq for thermally transferred samples and by 34.4% to 0.62 k Ω /sq for UV-transferred samples, offering a means of realising viable transparent flexible conductors that near the indium tin oxide benchmark.

1 Introduction

Graphene, a two-dimensional honeycomb of carbon atoms, has a myriad of novel optical and electrical properties [1, 2]. As such, it has attracted much attention as a promising material to complement indium and fluorine-based tin oxide in large-area transparent electronics for many applications including organic light emitting diodes [3–6], touch screens [5, 7, 8] and photovoltaic cells [9–11]. Graphene is mechanically flexible, does not readily form micro-cracks when strained and, when coupled with suitable substrates, provides an exciting and paradigm shifting technological platform for future flexible transparent electronic devices. Although mechanically and chemically exfoliated graphene and inks based thereon, have made some progress towards truly flexible, high form factor, transparent conductors, the intrinsic disorder and sub-micron grain sizes associated with such approaches limits their practicality [12–15]. Chemical vapour deposition (CVD) has thus supplanted exfoliation as the fabrication procedure of choice, particularly given recent technological advances and associated cost reductions in growth allowing for truly monolayer material of near-equivalent quality to mechanically exfoliated graphene with substantially higher yields [16–21]. Unlike exfoliated approaches, CVD graphene is large-area compatible and offers electrical continuity and optical uniformity without the use of aggressive chemical treatments. Nevertheless, for CVD graphene to be industrially viable, it must be transferred to arbitrary substrates from the optically opaque

catalyst on which the graphene was grown. Although the native properties of graphene are central to its function in a wide range of applications, the transfer method plays an equally important role in realising useful devices. Several transfer methods have been reported with hot and cold lamination being two such methods that have shown significant promise because of their facile processing, low-cost and large-area compatibility.

Polymers such as poly-methyl methacrylate (PMMA) and polydimethylsiloxane are commonly used to mediate the transfer process. Here, the polymer supports the graphene while the catalyst is etched [22–26]. The PMMA/graphene stack is then manoeuvred onto an arbitrary target substrate and the PMMA removed, typically in an acetone bath [22–27]. Although the value of this technique to the global research community is unrivalled, it lacks the fundamental commercial scalability required for an emerging material to gain industrial traction. Handling the polymer support, on areas greater than a few centimetres square, is challenging and requires significant training and associated expense [22, 28, 29]. Alternatives must be sought. In 2010, Bae *et al.* [5] transferred large-area CVD graphene using thermal release tape. Cu-foil-catalysed CVD graphene was attached to thermal release tape and the Cu etched in aqueous ammonium persulphate [(NH₄)₂S₂O₈]. The graphene was then transferred using a roll-to-roll system and the thermal release tape removed by heating to 100°C [5]. This approach allowed graphene transfer, layer-by-layer, onto arbitrary substrates. Nevertheless, this method cannot be applied to many low-cost and widely available polymeric

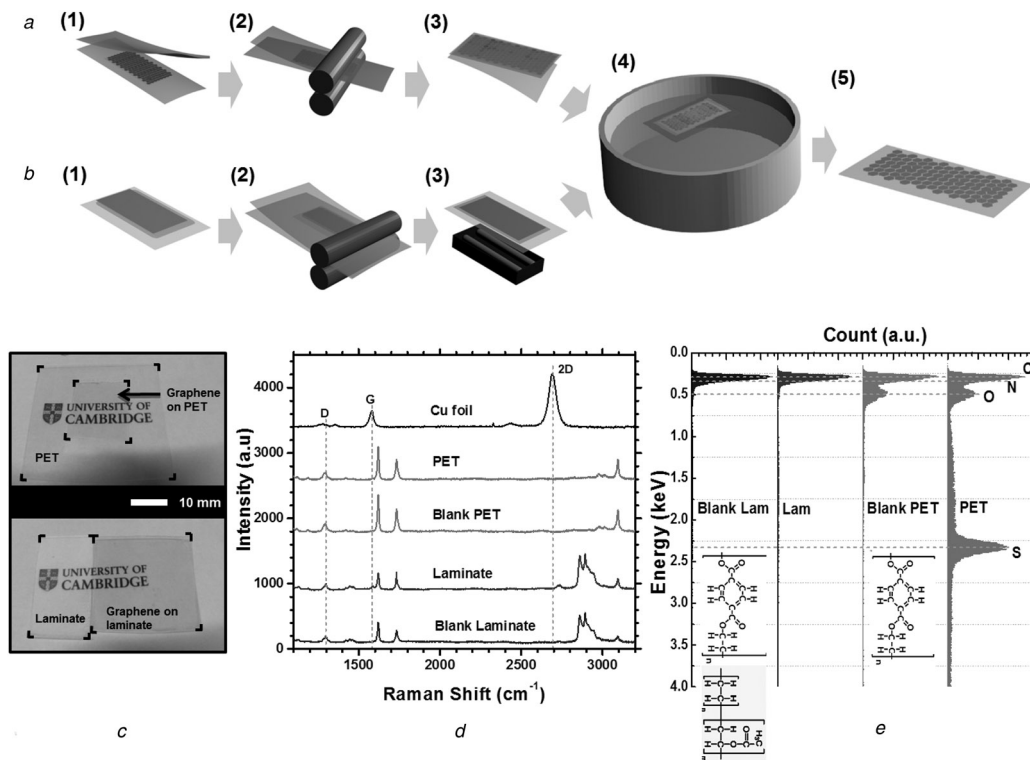


Fig. 1 Schematic depiction of

a Graphene transfer by thermal lamination

b Graphene transfer by UV-curable adhesive

c Optical images of graphene transferred on PET (top) and laminate (bottom) (scale bar: 10 mm)

d Raman spectra (457 nm) of the nascent Cu-foil-catalysed graphene by thermal CVD, as-received PET and laminate substrates and transferred graphene on PET and laminate

e EDX spectra of a blank laminate, a blank PET and transferred graphene on laminate and PET

substrates given the limited thermal budget of many such materials and the potentially high mismatch in thermal expansion coefficient which may induce crack formation, thereby compromising the films opto-electronic properties.

To overcome these drawbacks, we have investigated alternative transfer techniques and have studied the temporal variation of the opto-electronic properties of facile and mechanically stable thermal lamination and ultraviolet (UV)-curable adhesion transferred films.

At present, the sheet resistance (R_s) of single-layer graphene is of the order of a few $k\Omega/\text{sq}$; an order of magnitude too high to be an effective transparent conductive electrode in most applications. Chemical doping is considered the most appropriate means to decrease R_s without significantly compromising the optical transmission [30–36]. In this paper, we investigated the opto-electronic spatial uniformity and time-dependent behaviour of chemically doped polymer-supported graphene under ambient conditions following exposure to three common chloride-based dopants; ferric chloride (FeCl_3), tin chloride (SnCl_2) and gold chloride (AuCl_3).

2 Experimental results

Graphene was grown, as reported in detail elsewhere [37], using a commercially available Aixtron Black Magic Pro, hot-walled thermal CVD system on $25\ \mu\text{m}$ Cu foil (99.999% Alfa Aesar) under 5 sccm CH_4 (99.5%) at 1000°C in Ar: H_2 [960 (99.9997%): 40 (99.9992%) sccm] at 25 mbar. Following 15 min growth, samples were quenched under

2000 sccm N_2 (99.99%) to 250°C and were removed from the reactor. Graphene grains were $\sim 10\text{--}100\ \mu\text{m}$ in diameter with a mean area of $400\ \mu\text{m}^2$. Grains coalesced to form a large area, few layer polycrystalline graphene film. As-grown graphene was inspected by selected area electron diffraction (SAED) using an FEI Philips Tecnai operated at 200 keV. The SAED patterns were assessed relative to a thallium chloride calibration standard. Weak patterns from the supporting grid and residual organics were present. Six-fold symmetry, characteristic of the graphites and graphenes, was clearly noted. It is possible that the multiple, unassigned spots are associated with turbostratic alignment, although film discontinuity and polycrystallinity makes verification of this challenge. Certainly, the $\bar{1}010$ to $\bar{2}110$ intensity ratio ($I_{\bar{1}010}/I_{\bar{2}110}$) deviates somewhat from that of $A\text{--}A$ or $A\text{--}B$ (Bernal) stacking, suggesting a turbostratic multi-layered film [38–40].

To hot-press laminate the graphene-on-catalyst samples, commercially available thermally activated ethylene vinyl acetate treated polyethylene terephthalate (PET) substrates were used (GBC Co.). This hot-press lamination process, termed ‘laminate’ hereafter, is illustrated in Fig. 1*a*. First, graphene grown on Cu foil was sandwiched between two laminates (i) and passed through a dual roller laminator, heated to 120°C (ii). Following thermal lamination, the backside laminate was detached (iii) and the Cu etched in $(\text{NH}_4)_2\text{S}_2\text{O}_8$ in de-ionised (DI) water (1 M) for 12 h (iv). Following the etching, samples were rinsed with DI water and dried in high-purity N_2 (v). We have transferred areas of up to $10\ \text{cm} \times 10\ \text{cm}$ successfully using this method. Fig. 1*b* describes the UV-cured adhesive transfer approach.

The UV-curable adhesive was first coated onto acetone cleaned PET (i). The as-grown graphene on Cu was then placed on the adhesive and pressed at around 0.2 MPa, ensuring that all air was removed from the graphene-adhesive interface (ii). Plastic protective films were used to cover both sides of the Cu foil and the PET substrate. To cure the adhesive, the backside of the PET substrate was exposed to a UV optical source (365 nm, 222 Wm^{-2}) for 15 min (iii). Following optical curing, the Cu foil was etched in aqueous $(\text{NH}_4)_2\text{S}_2\text{O}_8$ for 12 h (iv), rinsed in DI water and dried in high-purity N_2 as before (v). Both transfer methods are rapid, inexpensive, large-area compatible and provide strong, long-lasting robust adhesion between the substrate and the graphene – critical for high form factor electronics. Fig. 1c shows typical optical micrographs of transferred samples.

3 Results

Fig. 1d shows a typical Raman spectrum (457 nm, Renishaw InVia) of the as-grown CVD graphene. The I_D/I_G ratio was 0.12 ± 0.05 suggesting a highly crystalline, well-graphitised material [41, 42] with an I_{2D}/I_G ratio of 2.33 ± 0.6 indicating bilayers. Repeated point measurements over large-areas suggested the presence, on average, of three to four layers [14, 41, 42]. The full-width at half-maximum (FWHM) of the 2D peak was narrow; $45\text{--}55 \text{ cm}^{-1}$, further suggesting high graphitisation [41, 42]. Additional spatially resolved Raman analysis, under 532 and 633 nm excitation, revealed a $\langle I_{2D}/I_G \rangle$ of 1.3–2.2, with the number of layers per unit area being relatively uniform with 79% coverage of three to four graphene layers, 14% bilayer and 7% monolayer. Raman spectra of the transferred graphene on laminate and PET showed no notable D, G or 2D peaks with the characteristic graphene spectra being indistinguishable from that of the polymer support. Nevertheless, energy-dispersive X-ray (EDX) analysis of the blank laminate, blank PET, graphene on laminate (laminate) and graphene on PET (PET) samples, as shown in Fig. 1e, evidences the distinct absence of any Cu suggesting that only the transferred carbon (C) from the as-grown graphene mediates the observed conductivity enhancement. The conductive carbon allotrope is most likely graphitic given the comparatively low transfer temperatures. EDX also revealed, in the case of the graphene on PET, significant sulphur (S) and oxygen (O) peaks, which we believe are most likely from the $(\text{NH}_4)_2\text{S}_2\text{O}_8$ exposure during the Cu-etch. Interestingly, such peaks were not observed for the laminate samples. Sulphur is a well-known potent dopant of graphitic nanocarbons [43, 44]. Evidently, the Cu etching produces significant unintentional, but nevertheless advantageous doping prior to any further chemical treatments.

Fig. 2a shows the optical transmittance spectra (%T) for graphene transferred to laminate and PET substrates (ATI, Unicam UV2). The transmittance (550 nm) of graphene on PET and on laminate was 10 and 12% lower than the as-received PET and laminate, respectively. The high optical absorption suggests around four layer coverage on average on for the PET samples and five layer coverage for the laminate [49, 50], broadly consistent with earlier Raman maps of the nascent material. As shown in Figs. 2b and c, the spatially averaged transmittance of the graphene/laminate and graphene/PET at 550 nm was 58.6 ± 3.6 and $76.5 \pm 3.8\%$, respectively. The PET transfer was around

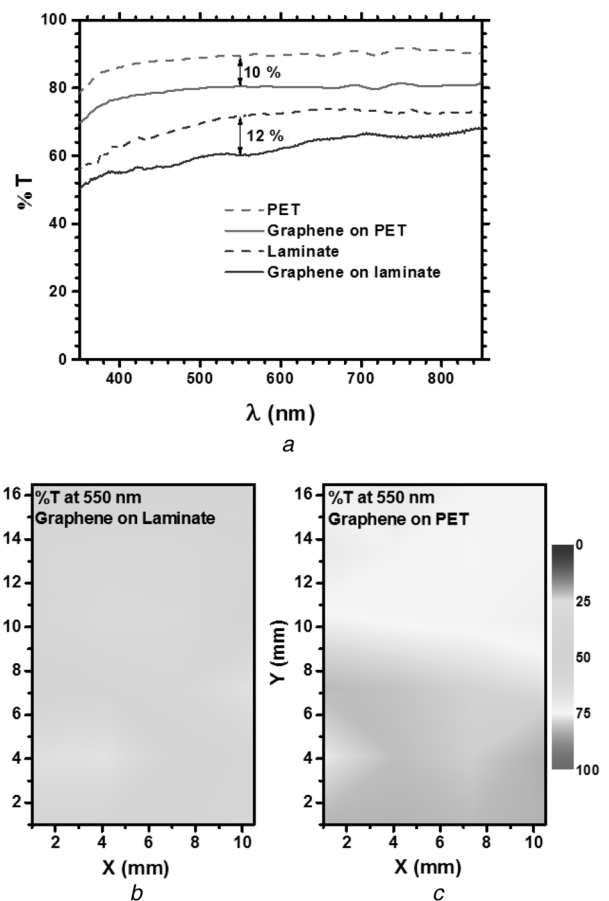


Fig. 2 Optical transmittance of polymer-supported graphene

a Typical optical transmittance spectra of graphene transferred to laminate and PET.

b Optical transmittance maps (550 nm) of graphene on laminate

c Optical transmittance maps (550 nm) of graphene on PET

18.1% more transparent than the laminate, although both transfer techniques afforded equivalent areal uniformity of $<4.0\%$ variation. The modest increase in absorption between the two samples is likely due to folding and wrinkling of the graphene during the transfer process, as clearly depicted in the scanning electron micrographs (SEM) (Hitachi, S4700SEM) of Figs. 3a and b and the atomic force microscopy (AFM) (Agilent, 5400SPM) in Figs. 3c and d. Certainly, hot-press lamination is more aggressive in terms of augmenting the morphology of the as-grown graphene. Indeed, the root mean square surface roughness of the graphene on the laminates was 161 nm, some 26% higher than the PET. The maximum perturbation for the graphene on laminate and PET was 949 nm and 551 nm, respectively. As eluded to prior, wrinkling increases the optical diffusivity but will, conversely, enhance the mechanical flexing performance of the electrodes.

Prior to the metal-chloride doping the sheet resistance for the as-grown graphene-laminate samples was $9.9 \pm 3.8 \text{ k}\Omega/\text{sq}$, whereas for the PET it was $3.5 \pm 2.3 \text{ k}\Omega/\text{sq}$ (Figs. 3e and f); PET samples showed a markedly lower R_s because of the notable sulphur doping. The growth and transfer process showed high reproducibility although some slight variation in sheet resistance and transmission between samples was observed. The sheet resistance of the as-grown graphene was assessed independently by transferring equivalent as-grown graphene to quartz substrates, using the conventional PMMA-approach, with subsequent Cr/Au Van der Pauw

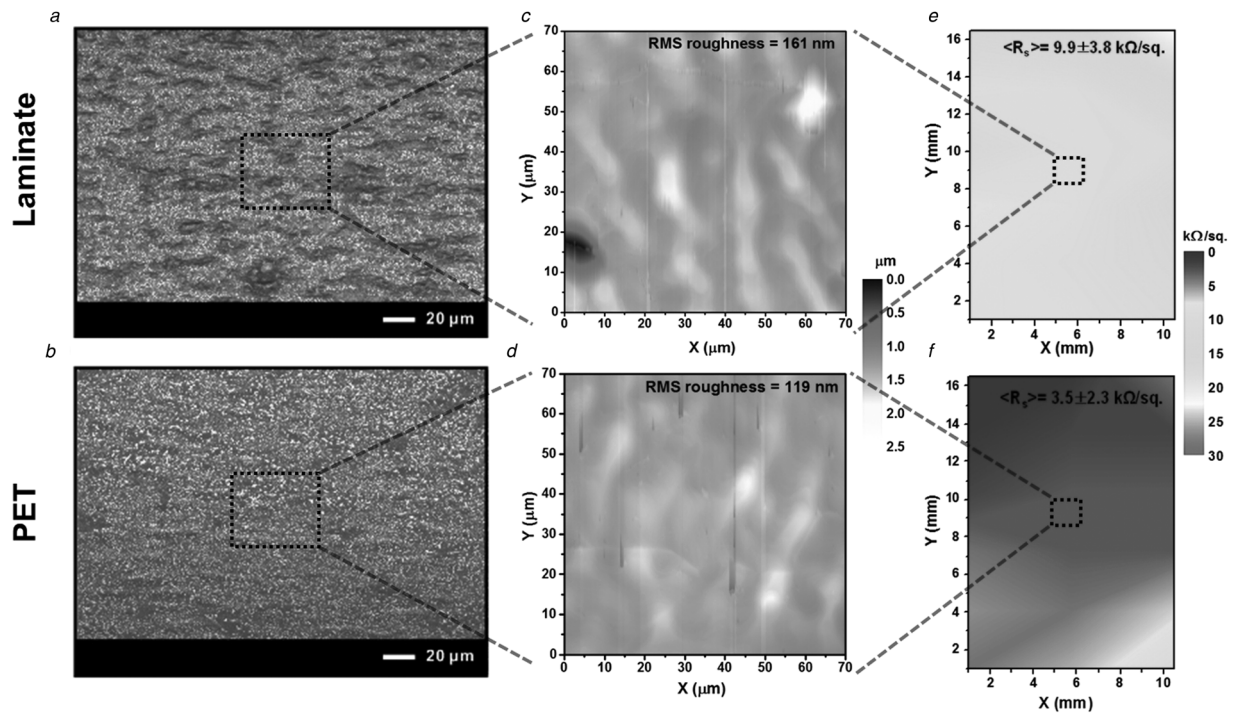


Fig. 3 Morphology and resistivity comparison

Scanning electron micrographs of the transferred graphene on
a Laminate
b PET (scale bar 20 μm)
 Atomic force micrographs of graphene on
c Laminate
d PET (scale bar 10 μm)
 Spatially resolved sheet resistance of graphene on
e Laminate
f PET

structures deposited by physical vapour deposition. This as-grown graphene had a sheet resistance of $5.47 \pm 1.20 \text{ k}\Omega/\text{sq}$. The laminate and UV-transferred samples showed an increase of around $4.43 \text{ k}\Omega/\text{sq}$ and, rather interestingly, a decrease of $1.97 \text{ k}\Omega/\text{sq}$ relative to the conventional PMMA-approach control sample, respectively. This decrease may be attributed to enhanced mass density and increased connectivity within the percolative network associated with significant wrinkling and augmentation of the as-grown morphology. Indeed, the transferred graphene on laminate and PET are non-contiguous. The agglomerates on the PET and laminate are $\sim 5.5 \pm 5.6 \mu\text{m}$ and $7.9 \pm 3.9 \mu\text{m}$ in diameter and are most likely adhesive residues.

Although stacking graphene to form artificial multi-layer materials is one possible way to decrease the sheet resistance, it has many intrinsic limitations; time and cost being but two. Alternatively, intentional chemical doping is one simple route to decrease the sheet resistance without the necessary complicated process and severe degradation of the optical transparency. In this paper, to reduce the sheet resistance to a technologically relevant value ($<0.3 \text{ k}\Omega/\text{sq}$), chemical doping via aqueous metal-chloride exposure of the UV and thermally transferred samples was investigated.

To assess the doping time stability, three common nanocarbon dopants were considered; FeCl_3 , SnCl_2 and AuCl_3 . FeCl_3 and SnCl_2 doping solutions were dissolved in DI water at 20 mM concentration. AuCl_3 was dissolved in nitromethane (20 mM). Laminate and PET samples were dipped into the dopant solutions for 5 min and dried with N_2 gas. For doping with AuCl_3 , as elsewhere [31, 33, 36],

the dopant solution was spin-coated at 2000 rpm for 1 min. Nitric acid (HNO_3), which has been previously reported as a *p*-type dopant [32, 34, 35], was also considered. However, the HNO_3 dissolved the adhesion layer in the PET samples resulting in the removal of the graphene. Adhesion in the laminate samples were unaffected by the HNO_3 and showed only a negligible decrease in R_s from 12.96 to $12.50 \text{ k}\Omega/\text{sq}$, while the %*T* decreased from 71.5 to 61.8%.

To assess the time evolution of the doping, the optical transmittance (550 nm) and sheet resistance were measured immediately after doping and at fixed time points thereafter, as illustrated in Figs. 4*a* and *b*, respectively. An ideal transparent conductor requires time and ambient invariant transmittance and sheet resistance. However, as reported elsewhere [31, 51], although dopants reduce the sheet resistance they also often reduce optical transmission, both of which notably shift deleteriously with time – an effect which is particularly exacerbated during ambient exposure. For all samples, the transmittance decreased following doping. The most significantly decreased transmittance (81 \rightarrow 54%) occurred for SnCl_3 -laminate, whereas FeCl_3 - and AuCl_3 -doped graphene showed smaller changes (FeCl_3 -laminate: 86 \rightarrow 77%, AuCl_3 -laminate: 81 \rightarrow 73%). A recovery process was noted with the transmittance tending to increase back to the undoped state. The most substantial increase was observed for the FeCl_3 -doped graphene (laminate: 77 \rightarrow 85%, PET: 60 \rightarrow 66%). This increase is presumed to be because of the time-dependent desorption of chemisorbed dopants, activated by ambient thermal

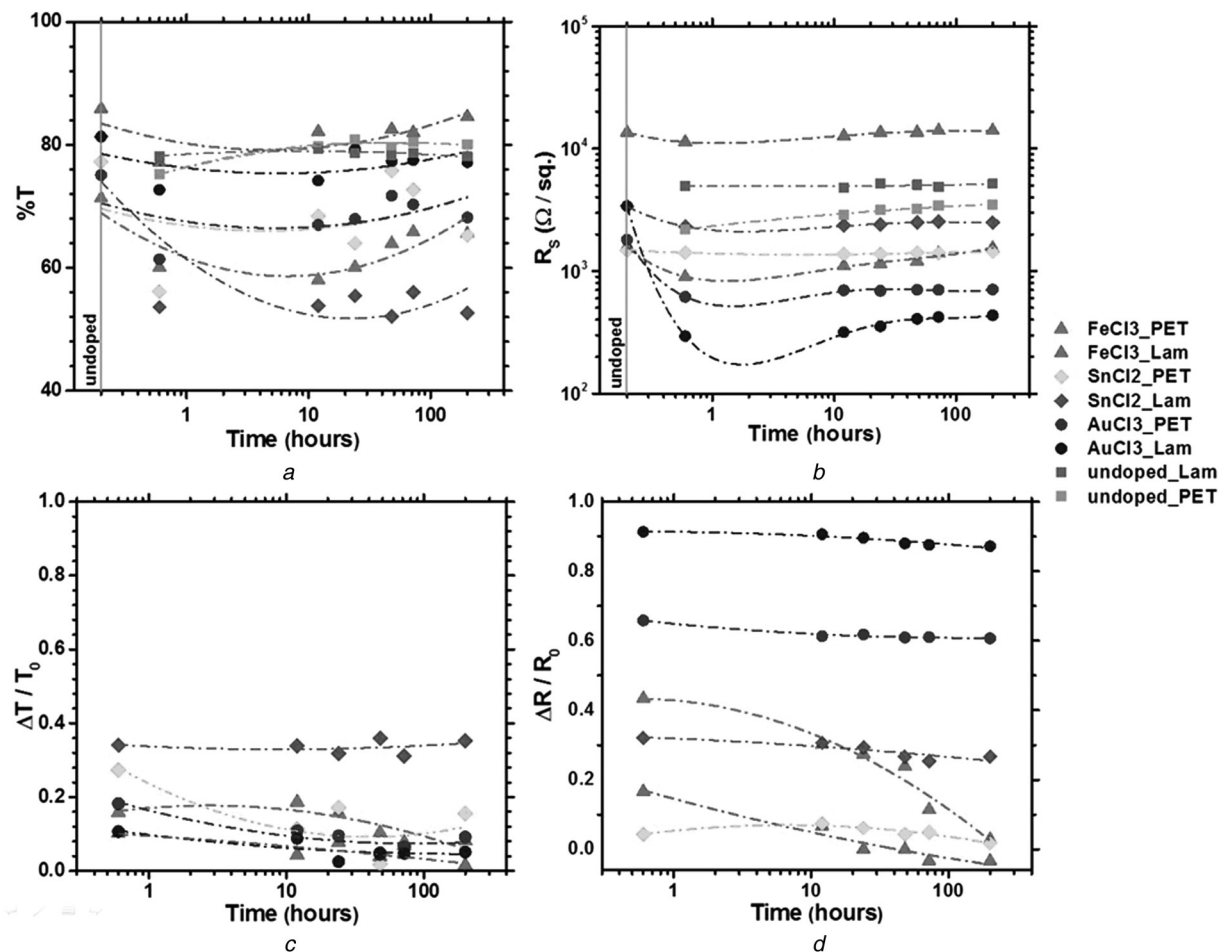


Fig. 4 Time-dependent electrical and optical properties of chemically doped graphene on laminate and PET substrates under ambient conditions

a Optical transmittance (% T)

b Sheet resistance (R_s) of doped graphene

c Ratio of the change in transmittance (ΔT) relative to the transmittance of undoped graphene (T_0)

d Ratio of sheet resistance relative to the sheet resistance of undoped graphene (R_0)

excitation [36, 45–48]. Interestingly, the transmittance of the undoped graphene on PET increased over time (75 → 80%), whereas there was no observable change for the graphene on laminate because of the absence of any significant doping during the transfer process, in contrast to the PET samples. It is unclear as to why the PET presented a higher inclination for sulphur binding than the laminate, although in order to fabricate a time-stable flexible transparent graphene-based electrode what is clear is that such transient binding must be prevented even though it reduces the initial sheet resistance. The metallic element within the chloride dopant is evidently central to the effectiveness and temporal stability of the observed doping; a detailed theoretical study of the underlying electron transport and its dependence on the metal type will be presented elsewhere. The ratio of the change in transmittance to the change in transmittance of the undoped graphene ($\Delta T/T_0$) is illustrated in Fig. 4c. $\Delta T/T_0$ for AuCl_3 and FeCl_3 was <0.1 at most time points highlighting the maintained optical quality of the doped films.

The undoped graphene on laminate showed a stable sheet resistance over time (5.0 → 5.2 k Ω /sq), while the undoped graphene on PET increased from an initial 2.2–3.5 k Ω /sq, after 200 h, again attributed to the unintentional sulphur

deposited during the graphene-transfer process. The AuCl_3 -doping dramatically reduced the sheet resistance from 3.4 to 0.29 k Ω /sq (laminate) and 1.8 to 0.62 k Ω /sq (PET). Nevertheless, as before, the sheet resistance in the AuCl_3 case still tended to increase with time, although to a much lesser extent, suggesting the need for polymer passivation or hermetic capping layers. $\Delta R/R_0$, the ratio of the change in sheet resistance of doped graphene to undoped graphene, is the highest for the AuCl_3 -laminate, as shown in Fig. 4d. Unlike the other dopants the reduced sheet resistance remains over time and only increased by 47% (laminate) and 15% (PET) after 200 h. The sheet resistance was as low as 294 Ω /sq for the AuCl_3 -laminate, which increased by only 141 Ω /sq, whereas for the AuCl_3 -PET it was 616 Ω /sq, and increased by only 92 Ω /sq after 200 h ambient exposure.

The ratio of the optical conductance, σ_{opt} , to the DC electronic conductance, σ_{dc} , defines a figure of merit of their opto-electronic performance, and can be estimated from

$$T = \left[1 + \left(\frac{tZ_0}{2} \right) \sigma_{\text{opt}} \right]^{-2} = \left[1 + 188.5 \frac{1}{R_s} \left(\frac{\sigma_{\text{opt}}}{\sigma_{\text{dc}}} \right) \right]^{-2} \quad (1)$$

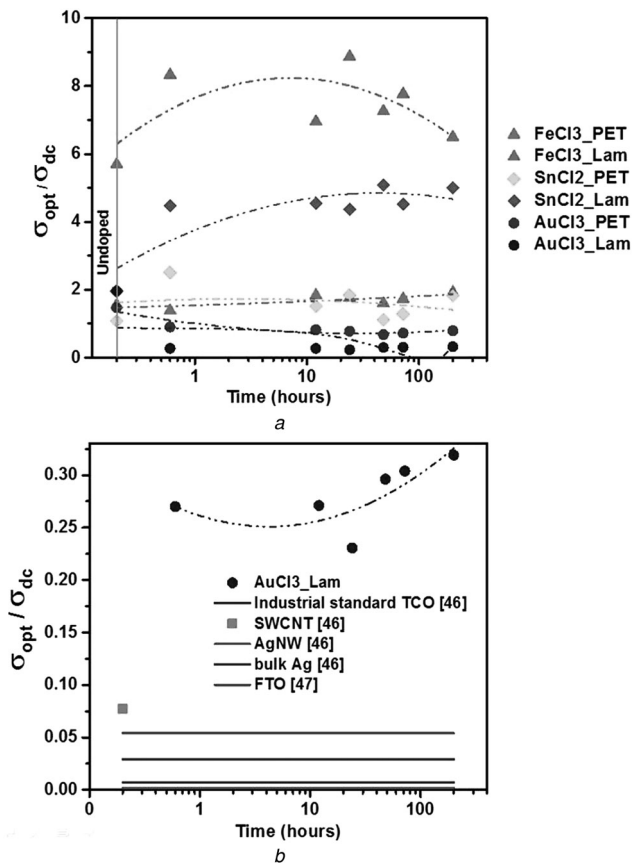


Fig. 5 Approximate σ_{opt}/σ_{dc} values of our transferred and doped graphene and other competing transparent flexible conductors

a Ratio of optical conductivity to dc electrical conductivity

b Comparison of the ratio to other conductive transparent media [52, 53]

Here Z_0 is the impedance of free space (377Ω) and t is the effective film thickness [53, 54]. For an ideal transparent conductive electrode $\sigma_{opt}/\sigma_{dc} \rightarrow 0$; requiring a low sheet resistance and high optical transmittance. The approximate σ_{opt}/σ_{dc} values of our transferred and doped graphene and other competing transparent flexible conductors are plotted in Figs. 5a and b, respectively. σ_{opt}/σ_{dc} was <2 for the FeCl₃-doped and SnCl₂-doped graphene cases and <1 for AuCl₃-doped graphene, during the entire measurement period (200 h; AuCl₃-laminated: 0.32 and AuCl₃-PET: 0.79). The conductivity ratio of AuCl₃-doped graphene on laminate is around ten times higher than the minimum industry standard (0.029), but was significantly lower than the undoped graphene and even lower again than that of stacked graphene (2.5) [54]. AuCl₃ doping is evidently a most efficient means to improve the opto-electronic conductivity of non-contiguous graphene on flexible and transparent substrates, and unlike other dopants, retains this state even after extended periods of time under ambient conditions.

4 Conclusion

Here, we have detailed techniques for thermal and cold lamination of graphene onto flexible and transparent substrates. High transfer fidelity, indicated by high spatial uniformity, homogenous optical transmission and sheet resistance were noted. Cold lamination using UV-curable adhesive produced less wrinkling of the nascent graphene relative to the hot lamination with the added benefit that in

the case of the cold lamination the films are doped with sulphur during the Cu-etch, reducing the sheet resistance without any additional doping processes. The reported facile transfer methods are inexpensive and reproducible. From time-dependent doping studies, we showed that AuCl₃ is a most effective dopant, even for non-contiguous thin films, giving sheet resistances as low as $294 \Omega/\text{sq}$ and a $\sigma_{opt}/\sigma_{dc} \sim 0.3$ after 200 h ambient exposure. Such facile-doped graphene/polymer films are showing increasing promise for highly transparent and highly conductive flexible electronics which may ultimately find use in organic light emitting diodes displays and next-generation photovoltaic devices.

5 Acknowledgments

M.T. Cole thanks the Winston Churchill Trust and the International Young Scientist Research Fellowship, National Natural Science Foundation of China, for generous financial support. We thank the Cavendish Laboratories, Cambridge University, for access to their Raman facilities and H.M. Tuncer, Cambridge University, for fruitful discussion.

6 References

- Novoselov, K.S., Geim, A.K., Morozov, S.V., *et al.*: 'Electric field effect in atomically thin carbon films', *Science*, 2004, **306**, (5696), pp. 666–669
- Zhang, Y., Tan, Y.W., Stormer, H.L., *et al.*: 'Experimental observation of the quantum hall effect and Berry's phase in graphene', *Nature*, 2005, **438**, (7065), pp. 201–204
- Kim, S.-Y., Kim, J.-J.: 'Outcoupling efficiency of organic light emitting diodes employing graphene as the anode', *Org. Electron.*, 2012, **13**, (6), pp. 1081–1085
- Wu, J., Agrawal, M., Becerril, H.A., *et al.*: 'Organic light-emitting diodes on solution-processed graphene transparent electrodes', *ACS Nano*, 2010, **4**, (1), pp. 43–48
- Bae, S., Kim, H., Lee, Y., *et al.*: 'Roll-to-roll production of 30-inch graphene films for transparent electrodes', *Nat. Nanotechnol.*, 2010, **5**, (8), pp. 574–578
- Han, T.-H., Lee, Y., Choi, M.-R., *et al.*: 'Extremely efficient flexible organic light-emitting diodes with modified graphene anode', *Nat. Photonics*, 2012, **6**, (2), pp. 105–110
- Lee, J., Cole, M.T., Lai, J.C.S., *et al.*: 'An analysis of electrode patterns in capacitive touch screen panels', *J. Disp. Technol.*, 2014, **10**, (5), pp. 362–366
- Jaeho, K., Masatou, I., Yoshinori, K., *et al.*: 'Low-temperature synthesis of large-area graphene-based transparent conductive films using surface wave plasma chemical vapor deposition', *Appl. Phys. Lett.*, 2011, **8**, (9), p. 091502
- Lin, P., Choy, W.C.H., Zhang, D., *et al.*: 'Semitransparent organic solar cells with hybrid monolayer graphene/metal grid as top electrodes', *Appl. Phys. Lett.*, 2013, **102**, (11), p. 113303
- Park, H., Brown, P.R., Bulovic, V., *et al.*: 'Graphene as transparent conducting electrodes in organic photovoltaics: studies in graphene morphology, hole transporting layers, and counter electrodes', *Nano Lett.*, 2012, **12**, (1), pp. 133–140
- Un Jung, Y., Na, S.-I., Kim, H.-K., *et al.*: 'Organic photovoltaic devices with low resistance multilayer graphene transparent electrodes', *J. Vac. Sci. Technol. A*, 2012, **30**, (5), p. 050604
- Park, S., Ruoff, R.S.: 'Chemical methods for the production of graphenes', *Nat. Nanotechnol.*, 2009, **4**, (4), pp. 217–224
- Wu, Y., Hao, Y., Jeong, H.Y., *et al.*: 'Crystal structure evolution of individual graphene islands during CVD growth on copper foil', *Adv. Mater.*, 2013, **25**, (46), pp. 6744–6751
- Torrissi, F., Hasan, T., Wu, W., *et al.*: 'Inkjet-printed graphene electronics', *ACS Nano*, 2012, **6**, (4), pp. 2992–3006
- Xu, K., Cao, P., Heath, J.R.: 'Scanning tunneling microscopy characterization of the electrical properties of wrinkles in exfoliated graphene monolayers', *Nano Lett.*, 2009, **9**, (12), pp. 4446–4451
- Zhou, H., Yu, W.J., Liu, L., *et al.*: 'Chemical vapour deposition growth of large single crystals of monolayer and bilayer graphene', *Nat. Commun.*, 2013, **4**, p. 2096

- 17 Yao, Y., Wong, C.-P.: 'Monolayer graphene growth using additional etching process in atmospheric pressure chemical vapor deposition', *Carbon*, 2012, **50**, (14), pp. 5203–5209
- 18 de la Rosa, C.J.L., Sun, J., Lindvall, N., *et al.*: 'Frame assisted H₂O electrolysis induced H₂ bubbling transfer of large area graphene grown by chemical vapor deposition on Cu', *Appl. Phys. Lett.*, 2013, **102**, (2), p. 022101
- 19 Celebi, K., Cole, M.T., Teo, K.B.K., *et al.*: 'Observations of early stage graphene growth on copper', *Electrochem. Solid-State Lett.*, 2012, **15**, (1), pp. K1–K4
- 20 Sun, J., Lindvall, N., Cole, M.T., *et al.*: 'Large-area uniform graphene-like thin films grown by chemical vapor deposition directly on silicon nitride', *Appl. Phys. Lett.*, 2011, **98**, (25), p. 252107
- 21 Celebi, K., Cole, M.T., Choi, J.W., *et al.*: 'Evolutionary kinetics of graphene formation on copper', *Nano Lett.*, 2013, **13**, (3), pp. 967–974
- 22 Kang, J., Shin, D., Bae, S., *et al.*: 'Graphene transfer: key for applications', *Nanoscale*, 2012, **4**, (18), pp. 5527–5537
- 23 Li, X., Cai, W., An, J., *et al.*: 'Large-area synthesis of high-quality and uniform graphene films on copper foils', *Science*, 2009, **324**, (5932), pp. 1312–1314
- 24 Kim, K.S., Zhao, Y., Jang, H., *et al.*: 'Large-scale pattern growth of graphene films for stretchable transparent electrodes', *Nature*, 2009, **457**, (7230), pp. 706–710
- 25 Suk, J.W., Kitt, A., Magnuson, C.W., *et al.*: 'Transfer of CVD-grown monolayer graphene onto arbitrary substrates', *ACS Nano*, 2011, **5**, (9), pp. 6916–6924
- 26 Hallam, T., Wirtz, C., Duesberg, G.S.: 'Polymer-assisted transfer printing of graphene composite films', *Phys. Status Solidi B*, 2013, **250**, (12), pp. 2668–2671
- 27 Cole, M.T., Hallam, T., Milne, W.I., *et al.*: 'Field emission characteristics of contact printed graphene fins', *Small*, 2014, **10**, (1), pp. 95–99
- 28 Liu, N., Pan, Z.W., Fu, L., *et al.*: 'The origin of wrinkles on transferred graphene', *Nano Res.*, 2011, **4**, (10), pp. 996–1004
- 29 Zhu, W., Low, T., Perebeinos, V., *et al.*: 'Structure and electronic transport in graphene wrinkles', *Nano Lett.*, 2012, **12**, (7), pp. 3431–3436
- 30 Dettlaff-Weglikowska, U., Skakalova, V., Graupner, R., *et al.*: 'Effect of SOCl₂ treatment on electrical and mechanical properties of single-wall carbon nanotube networks', *J. Am. Chem. Soc.*, 2005, **127**, (14), pp. 5125–5131
- 31 Gunes, F., Shin, H.J., Biswas, C., *et al.*: 'Layer-by-layer doping of few-layer graphene film', *ACS Nano*, 2010, **4**, (8), pp. 4595–4600
- 32 Kasry, A., Kuroda, M.A., Martyna, G.J., *et al.*: 'Chemical doping of large-area stacked graphene films for use as transparent, conducting electrodes', *ACS Nano*, 2010, **4**, (7), pp. 3839–3844
- 33 Shin, H.J., Choi, W.M., Choi, D., *et al.*: 'Control of electronic structure of graphene by various dopants and their effects on a nanogenerator', *J. Am. Chem. Soc.*, 2010, **132**, (44), pp. 15603–15609
- 34 Li, X., Xie, D., Park, H., *et al.*: 'Ion doping of graphene for high-efficiency heterojunction solar cells', *Nanoscale*, 2013, **5**, (5), pp. 1945–1948
- 35 Geng, H.-Z., Kim, K.K., Song, C., *et al.*: 'Doping and de-doping of carbon nanotube transparent conducting films by dispersant and chemical treatment', *J. Mater. Chem.*, 2008, **18**, (11), pp. 1261–1266
- 36 Hee Shin, D., Min Kim, J., Wook Jang, C., *et al.*: 'Annealing effects on the characteristics of AuCl₃-doped graphene', *J. Appl. Phys.*, 2013, **113**, (6), p. 064305
- 37 Li, C., Cole, M.T., Lei, W., *et al.*: 'Highly electron transparent graphene for field emission triode gates', *Adv. Funct. Mater.*, 2014, **24**, (9), pp. 1218–1227
- 38 Horiuchi, S., Gotou, T., Fujiwara, M., *et al.*: 'Carbon nanofilm with a new structure and property', *Jpn. J. Appl. Phys.*, 2003, **42**, (9ab), pp. L1073–L1076
- 39 Meyer, J.C., Geim, A.K., Katsnelson, M.I., *et al.*: 'The structure of suspended graphene sheets', *Nature*, 2007, **446**, (7131), pp. 60–63
- 40 Meyer, J.C., Geim, A.K., Katsnelson, M.I., *et al.*: 'On the roughness of single- and bi-layer graphene membranes', *Solid State Commun.*, 2007, **143**, (1–2), pp. 101–109
- 41 Ferrari, A.C., Meyer, J.C., Scardaci, V., *et al.*: 'Raman spectrum of graphene and graphene layers', *Phys. Rev. Lett.*, 2006, **97**, (18), p. 187401
- 42 Tang, B., Guoxin, H., Gao, H.: 'Raman spectroscopic characterization of graphene', *Appl. Spectrosc. Rev.*, 2010, **45**, (5), pp. 369–407
- 43 Denis, P.A., Faccio, R., Mombro, A.W.: 'Is it possible to dope single-walled carbon nanotubes and graphene with sulfur?' *Chemphyschem*, 2009, **10**, (4), pp. 715–722
- 44 Yang, Z., Yao, Z., Li, G., *et al.*: 'Sulfur-doped graphene as an efficient metal-free cathode catalyst for oxygen reduction', *ACS Nano*, 2012, **6**, (1), pp. 205–211
- 45 Kwon, K.C., Kim, B.J., Lee, J.-L., *et al.*: 'Effect of anions in Au complexes on doping and degradation of graphene', *J. Mater. Chem. C*, 2013, **1**, (13), pp. 2463–2469
- 46 Tongay, S., Berke, K., Lemaitre, M., *et al.*: 'Stable hole doping of graphene for low electrical resistance and high optical transparency', *Nanotechnology*, 2011, **22**, (42), p. 425701
- 47 Liu, H., Liu, Y., Zhu, D.: 'Chemical doping of graphene', *J. Mater. Chem.*, 2011, **21**, (10), pp. 3335–3345
- 48 Kwon, K.C., Kim, B.J., Lee, J.-L., *et al.*: 'Role of ionic chlorine in the thermal degradation of metal chloride-doped graphene sheets', *J. Mater. Chem.*, 2013, **1**, (2), pp. 253–259
- 49 Nair, R.R., Blake, P., Grigorenko, A.N., *et al.*: 'Fine structure constant defines visual transparency of graphene', *Science*, 2008, **320**, (5881), p. 13080
- 50 Mattevi, C., Kim, H., Chhowalla, M.: 'A review of chemical vapour deposition of graphene on copper', *J. Mater. Chem.*, 2011, **21**, (10), pp. 3324–3334
- 51 Ishikawa, R., Bando, M., Morimoto, Y., *et al.*: 'Doping graphene films via chemically mediated charge transfer', *Nanoscale Res. Lett.*, 2011, **6**, (1), p. 111
- 52 Rakhshani, A.E., Makhdisi, Y., Ramazaniyan, H.A.: 'Electronic and optical properties of fluorine-doped tin oxide films', *J. Appl. Phys.*, 1998, **83**, (2), pp. 1049–1057
- 53 De, S., Higgins, T.M., Lyons, P.E., *et al.*: 'Silver nanowire networks as flexible, transparent, conducting films: extremely high DC to optical conductivity ratios', *ACS Nano*, 2009, **7**, (3), pp. 1767–1774
- 54 De, S., King, P.J., Lotya, M., *et al.*: 'Flexible, transparent, conducting films of randomly stacked graphene from surfactant-stabilized, oxide-free graphene dispersions', *Small*, 2010, **6**, (3), pp. 458–464